Available online at www.sciencedirect.com

ScienceDirect

Energy Procedia 76 (2015) 582 – 591

Energy Procedia

European Geosciences Union General Assembly 2015, EGU

Division Energy, Resources & Environment, ERE

Thermo-mechanical simulations confirm: Temperature-dependent mudrock properties are nice to have in far-field environmental assessments of underground coal gasification

Christopher Otto[a,b,*], Thomas Kempka[a]

[a]GFZ German Research Centre for Geosciences, Section 5.3 – Hydrogeology, Telegrafenberg, 14473 Potsdam, Germany
[b]Institute of Earth and Environmental Science, University of Potsdam, Karl-Liebknecht-Str. 24-25, 14476 Potsdam, Germany

Abstract

Coupled thermo-mechanical simulations were carried out to quantify permeability changes in representative coal measure strata surrounding an underground coal gasification (UCG) reactor. Comparing temperature-dependent and -independent rock properties applied in our simulations, notable differences in rock failure behavior, but only insignificant differences in spatial permeability development are observed. Hence, temperature-dependent parameters are required for simulations of the close reactor vicinity, while far-field models can be sufficiently determined by temperature-independent parameters. Considering our findings in the large-scale assessment of potential environmental impacts of UCG, representative coupled simulations based on complex thermo-hydro-mechanical and regional-scale models become computationally feasible.

Peer-review under responsibility of the GFZ German Research Centre for Geosciences

Keywords: Underground coal gasification; thermo-mechanical modeling; temperature dependency, numerical simulation; environmental impacts

* Corresponding author. Tel.: +49-331-288-1865.
E-mail address: otto@gfz-potsdam.de

Peer-review under responsibility of the GFZ German Research Centre for Geosciences
doi:10.1016/j.egypro.2015.07.875

1. Introduction

1.1. Underground Coal Gasification (UCG)

UCG can increase world-wide coal reserves by utilization of coal deposits not mineable by conventional methods and has a long history [1]. The process of underground coal gasification is based on in situ, sub-stoichiometric coal combustion for production of a high-calorific synthesis gas, which can be applied for electricity generation or as chemical feedstock [2-7]. Fig. 1 presents a schematic view of the in-situ coal gasification principle using the Controlled Retraction and Injection Point (CRIP) configuration [8]. However, UCG can induce environmental impacts such as ground subsidence and groundwater pollution [6,9-12]. Changes in the hydraulic conductivity of the hanging wall may generate potential pathways for UCG contaminant migration [13-16]. These changes are associated with mechanical stress changes resulting from the UCG reactor growth as well as thermal stresses [17]. Permeability controls fluid in- and outflow into and out of the reactor, respectively, considering the pressure gradient between the hydrostatic fluid and UCG reactor operating pressure [18-20]. Mitigation of potential environmental UCG impacts can be achieved by improving the understanding of coupled thermo-hydro-mechanical processes in the rocks surrounding the UCG reactor at different scales. Thereby, near-field models considering the close UCG reactor vicinity can be employed to represent temperature-dependent processes, while far-field models are required to assess environmental impacts at regional scale. However, far-field models become computationally expensive, if processes taking place in the close reactor vicinity are involved, especially in the assessment commercial-scale multi-channel UCG operations.

Hence, a coupled thermo-mechanical model has been developed in the scope of the present study to assess near-field temperature-dependent and -independent rock behavior and permeability changes in mudrocks as previously carried out for a sandstone based coal measure strata [21].

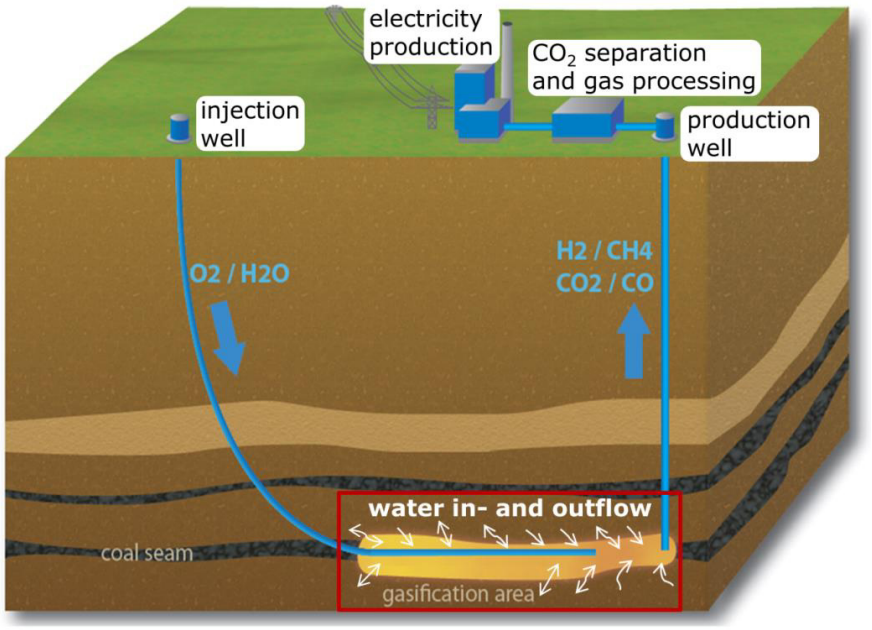

Fig. 1. Principle of in situ coal gasification based on the CRIP method (modified after [8]).

2. Methodology

2.1. Numerical model geometry and boundary conditions

The model used in the present study has been introduced by Otto and Kempka [21] for simulation of UCG processes considering, thermo-mechanical coal and sandstone properties. To assess these simulation results in view of a different host rock type, thermo-mechanical material properties of claystone and mudstone, hereafter called mudrock, were implemented into the given numerical model.

The size and grid discretization of the numerical model were adapted to calculation time and the impact of the chosen boundary conditions on the simulation results. The implemented numerical model uses the UCG reactor symmetry present along its vertical axis, assuming that a half-radial symmetric reactor develops along the UCG panel (Fig. 2). The two-dimensional geometry of a coal seam of 4 m thickness was uniformly expanded towards the model boundaries, with the reactor bottom located at a depth of 250 m below the ground surface. The model size was set to 40 m × 110 m and discretized by about 3,000 elements, with sizes of 0.16 m to 5 m in all directions.

The finite-difference thermo-hydro-mechanical simulator FLAC3D [22] was employed to analyze thermos-mechanical stress changes, displacements and volumetric strain increments in the UCG reactor vicinity, using the unstructured grid presented in Fig. 2.

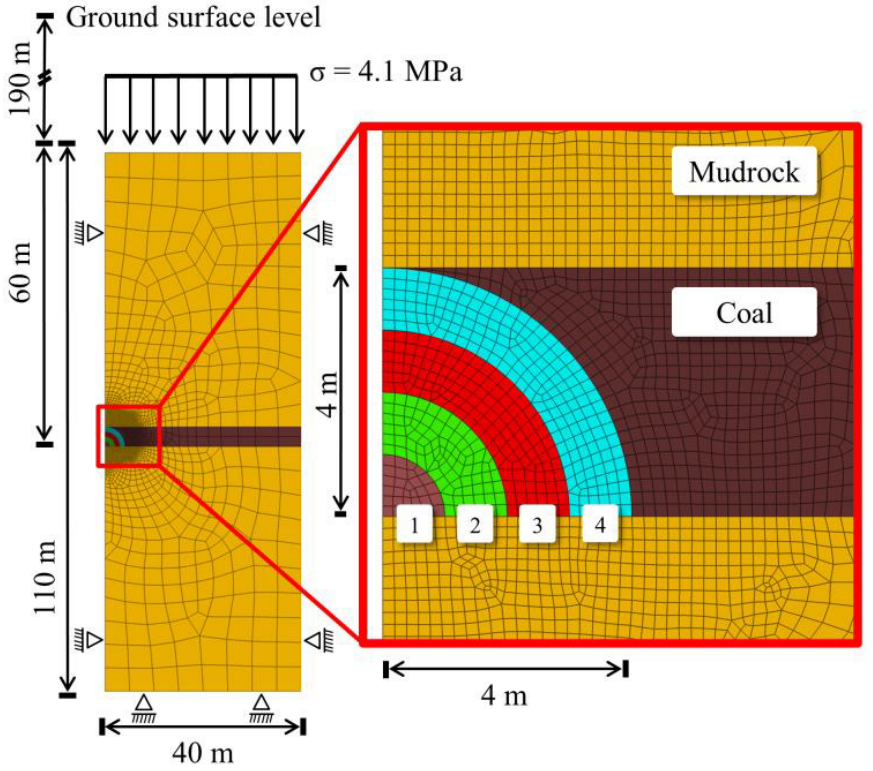

Fig. 2. Geometry of the coupled thermal-mechanical UCG model. The model comprises two mudrock layers (colored in light brown) and one coal seam (colored in dark brown) with four geometric reactor growth steps considered in the simulations (light brown, green, red and turquois) (modified after [21]).

2.2. Model parameterization and material properties

Thermo-mechanical data on claystone and mudstone specimens exposed to high temperatures were derived from literature [23-26]. We incorporated both rock-type properties in one rock layer (mudrock), since the available data on thermo-mechanical properties of pure claystone and mudstone is limited. Temperature dependent thermo-mechanical properties of mudrock assigned to the present model include the elastic modulus (E), cohesion (c), friction angle (φ), linear thermal expansion coefficient (α), specific heat capacity (C_P) and thermal conductivity (λ) (Fig. 3).

In contrast to sandstone, whose elastic modulus generally decreases with increasing temperature [27], Tian et al. [23] found that the trend is slightly increasing for claystone (at 5 MPa confining pressure), what is in good agreement with the experimental results presented by Wolf et al. [28]. The normalized trends of friction angles and cohesion of the claystone specimens after high temperature treatment are always higher than those at room temperature, but also strongly alternating with increasing temperature [24].

Temperature-dependent thermal properties for the linear thermal expansion coefficient, specific heat capacity and thermal conductivity are not yet experimentally determined for claystone [23]. In this study, the normalized trends of mudstone properties are used in the model instead. Tan et al. [26] reported that the linear thermal expansion coefficient of mudstone increases in a continuous linear manner, until a temperature of 575 °C is reached. This is due to the α–β quartz phase inversion as reported also for other sedimentary rocks [29]. Thereafter, the linear thermal expansion coefficient is slightly decreasing up to temperatures of 1,000 °C. In accordance with other studies on sedimentary rocks [30], Tang et al. [25] reported a generally decreasing trend in thermal conductivity with increasing temperature for mudstone. Furthermore, the test results of Tang et al. [25] show that both, the specific heat capacity and the thermal conductivity, decrease with the increase in temperature when the testing temperature is below 400 °C. The specific heat capacity is almost constant and the thermal conductivity still continues to decrease for testing temperatures above 400 °C [25].

The claystone density (ρ) [28] and the Poisson's ratio (v) for mudstone [26] was maintained constant for both geological units (coal and mudrock). The tensile strength of claystone (0.19 MPa) was also taken from Wolf et al. [28] and maintained constant with increasing temperature for the mudrock. Min [31] reported a generally decreasing trend of the tensile strength of rock (oil shale and igneous rocks) with increasing temperature; however, no data for claystone or mudstone are yet available.

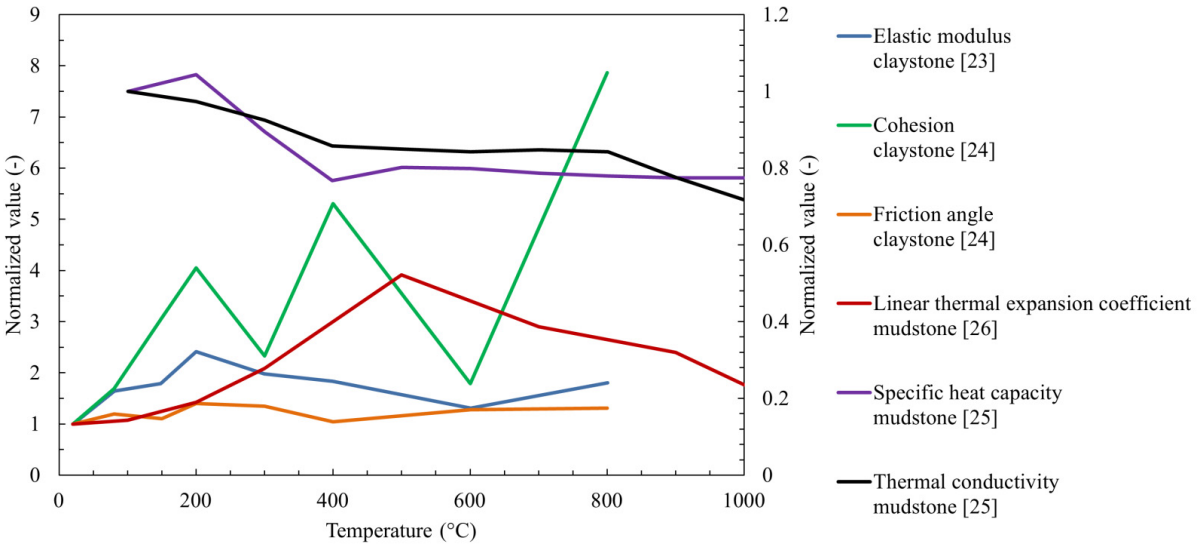

Fig. 3. Trend of normalized thermo-mechanical properties of claystone and mudstone as a function of temperature. The normalized values of specific heat capacity and thermal conductivity are plotted on the secondary vertical axis. All data are normalized using the initial values presented in Table 1.

The normalized trends of thermo-mechanical coal properties after high temperature treatment are derived from literature [31-34] and discussed in Otto and Kempka [21]. Changes in thermo-mechanical material properties affecting the coal behavior are mainly related to the various reactions in the different temperature zones [10]: the drying zone (up to 200 °C), the drying and pyrolysis zone (200-900 °C), the reducing zone (550-900 °C) and oxidation zone (above 900 °C).

Temperatures above 1,500 °C can be achieved in the UCG reactor and its close vicinity. However, the maximum testing temperature of the properties used in the present study is limited to 800 °C for the mechanical and 1,000 °C for the thermal material properties. Hence, an overall temperature limit of 1,000 °C is applied in the present simulations. The initial model parameters are presented in Table 1.

Table 1. Initial thermo-mechanical rock properties applied for model parameterization.

Input parameter		Unit	Mudrock	Coal
Mechanical parameters				
Young's modulus (E)	*f(T)*	GPa	2.1	2
Tensile strength (σ_t)	*Constant for rock, f(T) for coal*	MPa	0.19	0.275
Friction angle (φ)	*f(T)*	°	32.19	20
Cohesion (c)	*f(T)*	MPa	1.51	0.1
Poisson's coefficient (ν)	*Constant rock and coal*	-	0.23	0.44
Density (ρ)	*Constant rock and coal*	kg/m³	2,300	1,300
Thermal parameters				
Linear thermal expansion coefficient (α)	*f(T)*	K^{-1}	7.92×10^{-6}	5.0×10^{-6}
Specific heat capacity (C_P)	*f(T)*	J/(kg K)	1,187	2,000
Thermal conductivity (λ)	*f(T)*	W/m/K	1.19	0.23

2.3. Deriving permeability changes from volumetric strains

In the present study, the approach discussed and introduced by Otto and Kempka [21] is applied, where deformation is associated with volume changes affecting the host rock and coal permeability. The rock compaction behavior in the UCG reactor vicinity was simulated using an isotropic elastoplastic constitutive law with the material properties shown in Table 1. For modeling thermal and mechanical stress-induced permeability changes, permeability is related to volumetric strain increments [35]:

$$\phi = 1 - (1 - \phi_1) e^{-\Delta \varepsilon_v} \tag{1}$$

$$k = k_i \left(\frac{\phi}{\phi_1} \right)^n \tag{2}$$

where ϕ is the porosity at a given volumetric strain ε_v, ϕ_i the initial porosity, k the permeability at a given ε_v, k_i the initial permeability, and n a power-law exponent (porosity sensitivity exponent) with a value range of 2 to 25 depending on stress and lithology [36].

2.4. Scenario analysis

Simulations of coupled thermo-mechanical processes for a UCG process duration of 50 days were carried out in two steps. First, the initial model is run to achieve a mechanical equilibrium and then applied as starting model for all further simulations. The UCG reactor is excavated stepwise, depending on the pre-defined coal consumption rate (0.654 t/day/m). A constant temperature of 1,000 °C is applied at the reactor boundary, while the model is calculated to mechanical equilibrium after each reactor slice excavation. The temperature-dependent rock and coal properties are updated for each element during the entire simulation.

3. Simulation results

3.1. Principal stress distribution

During the UCG process, the experienced high temperatures generate a high thermal gradient of limited spatial extent for temperature-dependent as well as -independent material properties, and thus induce thermal stresses in the surrounding rock mass. Rock strength and behavior under high temperatures differ from those at initial conditions (Fig. 3). In both simulations, the maximum distance of the 200 °C isotherm to the reactor boundary is almost identical (Fig. 4). However, the temperature-dependent simulation results exhibit a significantly larger spatial distribution of tensile stresses in the reactor vicinity.

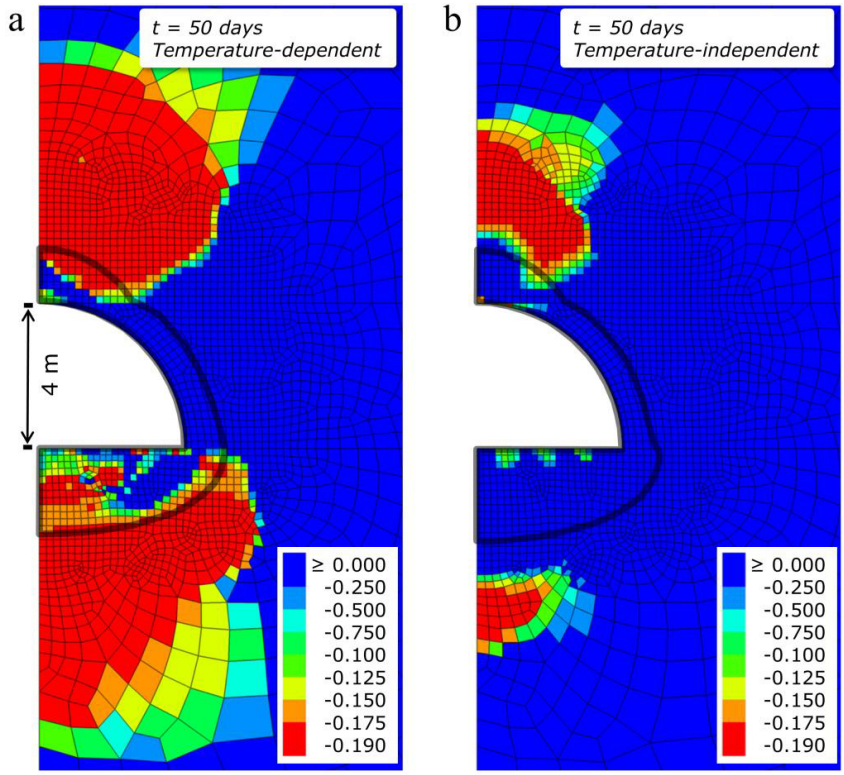

Fig. 4. Tensile minimum principal stress (in MPa) with (a) temperature-dependent and (b) -independent properties after 50 days of simulation. The grey solid line represents the 200 °C isotherm. Blue colors indicate compressive stresses.

3.2. Elastoplastic rock behavior

Shear and tensile failure determined by the Mohr-Coulomb failure criterion occur at multiple locations in the reactor vicinity considering temperature-dependent and -independent properties due to excavation effects and thermally-induced stresses (Fig. 5). Shear and tensile failure (green) dominate at the reactor wall, followed by a region of pure tensile failure (blue) above and below the reactor. The radius of tensile failure in the over- and underburden around the reactor is notably larger (up to 6 m) in the simulation using temperature-dependent parameters. The coal seam mainly experiences shear failure (red) in both models. The region of shear failure is determined by stress changes induced by excavation effects.

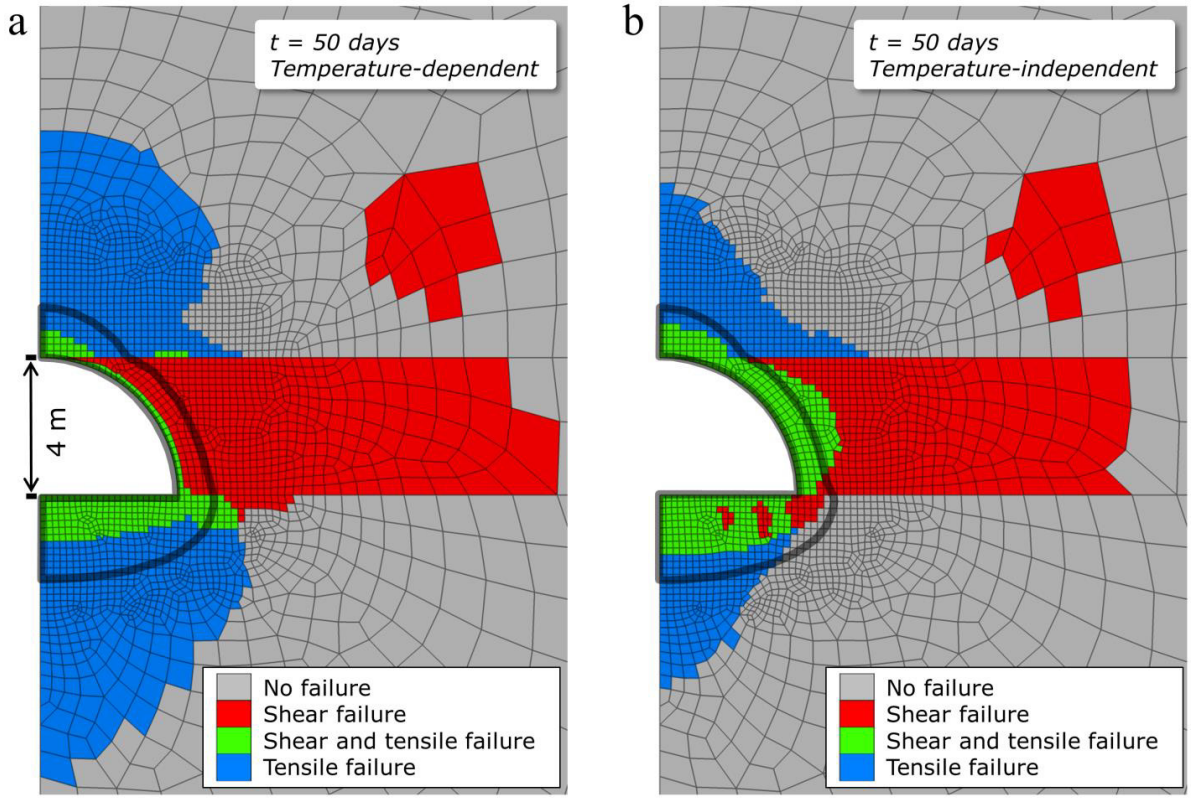

Fig. 5. Distribution of shear and tensile rock failure experienced by rocks surrounding the UCG reactor after stepwise reactor zone excavation with (a) temperature-dependent and (b) -independent properties after 50 days of simulation. The grey solid line represents the 200 °C isotherm.

3.3. Permeability changes

Equation 2 is applied for calculating permeability changes in the present models. For that purpose, normalized permeabilities with an initially uniform distribution and rock-specific porosity values derived from literature were applied (Table 2).

Table 2. Initial averaged data applied in the permeability change analysis [21,23,31].

Initial Values	Coal	Mudrock
ϕ_i	0.02	0.0875
Normalized k_i	1	1
n	13	13

Simulation results indicate that the maximum permeability increase by more than one magnitude (red elements) is located around the UCG reactor at a distance of up to 2 m for the temperature-dependent and up to 0.8 m for the temperature-independent simulations (Fig. 6). The area affected by increased permeability above the UCG reactor is notably larger for the temperature-dependent simulation; however, normalized permeability changes in that area in comparison between both simulation cases do not exceed a factor of three. Permeability increases in the temperature-dependent simulation are mainly mechanically induced and in good agreement with the larger region of tensile failure plotted in Fig. 5.

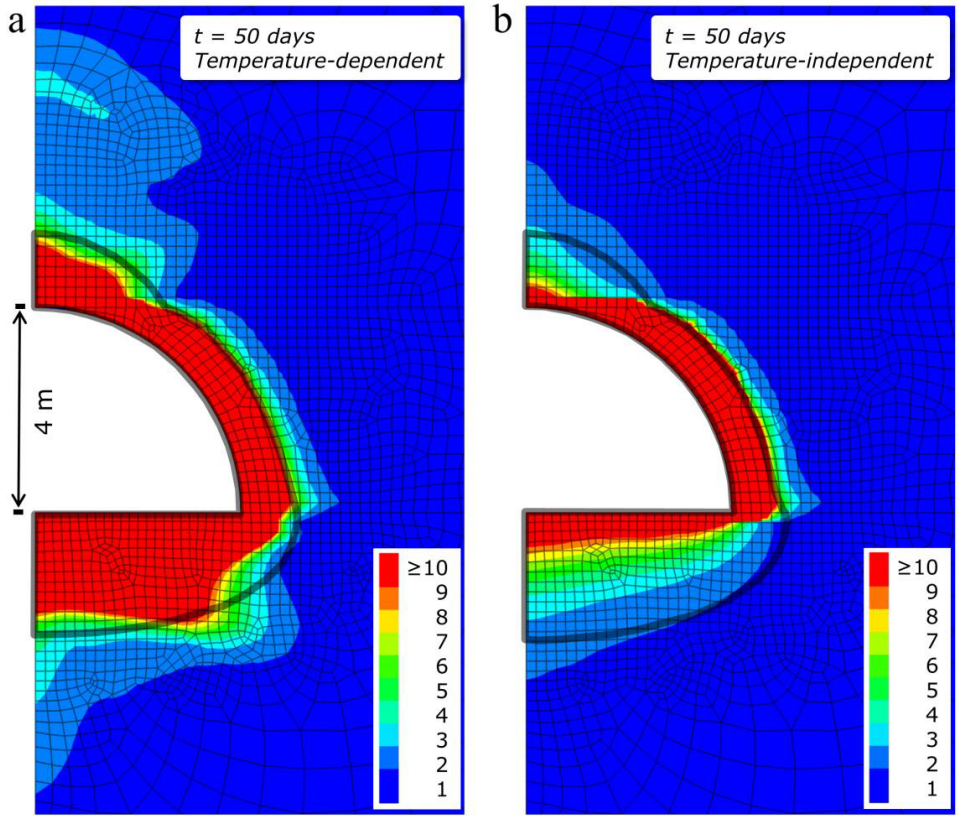

Fig. 6. Permeability changes (-) show small differences for temperature-dependent (a) and temperature-independent parameters (b). The difference in regions of high permeability increase is only marginal. The grey solid line represents the 200 °C isotherm.

4. Discussion and Conclusion

To investigate the impact of temperature-dependent parameters on rock behavior and permeability changes around a hypothetical UCG reactor, we compared coupled thermo-mechanical simulation results with temperature-dependent and -independent claystone and mudstone parameters. For the thermo-mechanical numerical

model, published data from high-temperature experimental results was implemented, comprising three geological units as discussed in Otto and Kempka [21]. The UCG reactor excavation was carried out stepwise, whereby a constant temperature of 1,000 °C was permanently applied at the reactor wall to represent the heat flux generated by in situ coal combustion.

Tensile and shear failure in the rocks surrounding the UCG reactor occur in a radius of up to 6 m in the temperature-dependent and -independent simulations. The associated volumetric strains result in significant permeability changes in the close reactor vicinity. For determination of permeability changes, we applied proven relationships between volumetric strain increments, porosity and permeability. Even though the formation of fractures is not considered in our simulations, the calculated volumetric strain increments achieve maximum values of up to 36 %, resulting in a permeability increase by more than three magnitudes in the high-temperature regions close to the UCG reactor (>200 °C).

Tensile failure dominates in the rocks close to the reactor in the temperature-dependent simulation. Compared to the simulations results using sandstone properties [21], the radial extent of tensile failure is notably higher (up to about 6 m in the present study compared with about 2 m). The main reason for these deviations is the lower value of tensile strength of claystone (0.19 MPa) compared with sandstone (5 MPa) [21]. Further, we expect the high alternations in the integrated temperature-dependent friction and cohesion data to contribute to this behavior.

A model verification against laboratory or field data on measured porosity and permeability changes is not yet feasible due to limited data availability. David et al. [36] and Chin et al. [35] developed the formulations applied here for the calculation of porosity and permeability changes for different porous and metamorphic rocks using laboratory experiments. However, we expect that the conceptual approach is applicable to the mudrock used in the present study, since a general increase in permeability due to baking, shrinking and fracturing effects is documented for rocks affected by high temperatures as experienced during in situ coal combustion [17]. In general, any porosity and permeability relationship determined at laboratory or field scale can be easily implemented in the presented models.

Our simulation results demonstrate that the temperature-dependent thermo-mechanical properties have a notable influence on stress changes and deformation around the UCG reactor. In the close reactor vicinity, the deformations induce positive volumetric strains and zones of high permeability (up to three magnitudes increase). However, permeability changes calculated based on volumetric strain increments show only small differences between simulations using temperature-dependent and -independent parameters for the representative coal measure strata investigated here. Hence, our results support our previous findings [21], emphasizing that near-field thermos-mechanical UCG simulation models require temperature-dependent parameters, while far-field 3D models can benefit from neglecting temperature-dependency to increase computational efficiency.

Acknowledgements

The authors gratefully acknowledge the funding received in the EU-FP7 TOPS project (grant 608517) funded by the European Union (EU).

References

[1] Klimenko AY. Early Ideas in Underground Coal Gasification and Their Evolution. Energies 2009; 2: 456-476.
[2] Nakaten NC, Schlüter R, Azzam R, Kempka T. Development of a techno-economic model for dynamic calculation of cost of electricity, energy demand and CO2 emissions of an integrated UCG–CCS process. Energy 2014; 66: 779-790.
[3] Nakaten NC, Kötting P, Azzam R, Kempka T. Underground Coal Gasification and CO2 Storage Support Bulgaria's Low Carbon Energy Supply. Energy Procedia 2013; 40: 212-221.
[4] Bhutto AW, Bazmi AA, Zahedi G. Underground coal gasification: From fundamentals to applications. Prog. Energy Combust. Sci. 2013; 39: 189-214.
[5] Blinderman MS, Saulov DN, Klimenko AY. Forward and reverse combustion linking in underground coal gasification. Energy 2008; 33: 446-454.
[6] Burton E, Friedmann J, Upadhye R. Best practise in underground coal gasification. Technical Report. CA: Lawrence Liveromore National Laboratory, US Department of Energy; 2006.
[7] Friedmann SJ, Upadhye R, Kong FM. Prospects for underground coal gasification in carbon-constrained world. Energy Procedia 2009; 1:4551-4557.

[8] Sarhosis V, Yang D, Sheng Y, Kempka T. Coupled Hydro-thermal Analysis of Underground Coal Gasification Reactor Cool Down for Subsequent CO2 Storage. Energy Procedia 2013; 40:428-436.
[9] Durucan S, Korre A, Shi JQ, Idiens M, Stańczyk K, Kapusta K, et al. TOPS: Technology Options for Coupled Underground Coal Gasification and CO2 Capture and Storage. Energy Procedia 2014; 63:5827-5835.
[10] Couch GR. Underground Coal Gasification. CCC/151 IEA Clean Coal Centre, John Topper, London, United Kingdom; July 2009.
[11] Sury M, White M, Kirton J, Carr P, Woodbridge R, Mostade M, et al. Review of Environmental Issues of Underground Coal Gasification. WS Atkins Consultants Ltd., University of Liège Belgium, FWS Consultants Ltd., 126. Report No. COAL R272 DTI/Pub URN 04/1880; 2004. p. 1-126.
[12] Hewing G, Hewel-Bundermann H, Krabiell K, Witte P. Post-1987 R&D Studies of Underground Coal Gasification. Research Association for Second-Generation Coal Extraction: Essen, Germany; 1987.
[13] Kapusta K, Stańczyk K. Pollution of water during underground coal gasification of hard coal and lignite. Fuel 2011; 90: 1927-1934.
[14] Liu S, Li J, Mei M, Dong D. Groundwater Pollution from Underground Coal Gasification. J. China Univ. Min. Technol. 2007; 17: 467-472.
[15] Walters EA, Niemczyk TM. The Effect of Underground Coal Gasification on Ground Water. US EPA. EPA-600/S2-84-123, Lawrence Livermore National Lab: Livermore, CA, USA; 1984.
[16] Humenick MJ, Mattox CF. Groundwater pollutants from underground coal gasification. Water Res. 1978; 12: 463-469.
[17] Wolf KH, Bruining H. Modelling the interaction between underground coal fires and their roof rocks. Fuel 2007; 86: 2761-2777.
[18] Seifi M, Abedi J, Chen Z. Application of porous medium approach to simulate UCG process. Fuel 2014; 116: 191-200.
[19] Seifi M, Abedi J, Chen Z. Numerical simulation of Underground coal gasification using the crip method. Can. J. Chem. Eng. 2011; 89: 1528-1535.
[20] Blinderman MS, Anderson B. Underground coal gasification for power generation: Efficiency and CO2-emissions. In Proceedings of the 12th International Conference on Coal Science, Cairns, Australia, 2–6 November 2003.
[21] Otto C, Kempka T. Thermo-mechanical simulations of rock behavior in underground coal gasification show negligible impact of temperature-dependent parameters on permeability changes. Energies 2015; 8: 5800-5827.
[22] Itasca. FLAC3D Software Version 5.01. User's Manual. Advanced Three-Dimensional Continuum Modelling for Geotechnical Analysis of Rock, Soil and Structural Support; 2013.
[23] Tian H, Ziegler M, Kempka T. Physical and mechanical behavior of claystone exposed to temperatures up to 1000 °C. Int. J. Rock Mech. Min. Sci. 2014; 70: 144-153.
[24] Tian H. Development of a Thermo-Mechanical Model for Rocks Exposed to High Temperatures during Underground Coal Gasification. Ph.D. Thesis, RWTH Aachen University, Aachen, Germany, 8 May 2013.
[25] Tang F, Wang L, Lu Y, Yang X. Thermophysical properties of coal measure strata under high temperature. Environmental Earth Sciences, May 2015; 73(10): p. 6009-6018.
[26] Tan Q, Luo X, Li S. Numerical modeling of thermal stress in a layered rock mass. In Proceedings of the 42nd US Rock Mechanics Symposium and 2nd U.S.–Canada Rock Mechanics Symposium, San Francisco, CA, USA, 29 June–2 July 2008.
[27] Tian H, Kempka T, Xu NX, Ziegler M. Physical Properties of Sandstones After High Temperature Treatment. Rock Mechanics and Rock Engineering 2012; 45(6):1113-1117.
[28] Wolf KHAA, Hettema MHH, de Pater CJ, van Hooijdonk R. Classification of overburden properties for underground coal gasification: laboratory studies under high temperature and in situ stress conditions. Proceedings of the ISRM Symposium: Eurock '92, International Society of Rock Mechanics, September 1992, Chester, UK, ISBN 0-7277-1688-3, T. Telford, London, 1992. p. 99-104.
[29] Somerton WH. Thermal Properties and Temperature Related Behavior of Rock/Fluid Systems. In Developments in Petroleum Science, 37, Chilingarian, G.V., Ed.; Elsevier: Amsterdam, The Netherlands; 1992.
[30] Clauser C, Huenges E. Thermal conductivity of rocks and minerals. In Thermal Conductivity of Rocks and Minerals ROCK Physics and Phase Relations: A Handbook of Physical Constants. Ahrens, T.J., (eds.) Washington, DC, USA, 1995; p. 105-126.
[31] Min OK. Finite Element Modeling of Thermo-Mechanical Responses Associated with Underground Coal Conversion. Ph.D. Thesis, Ohio State University, Columbus, OH, USA; 1983.
[32] Shoemaker HD, Shuck LZ, Haynes RR, Advani SH. The mechanical properties of the Pittsburgh coal at elevated temperatures. J. Press. Vessel Technol. 1977; 99: 192-198.
[33] Singer JM, Tye RP. Thermal, Mechanical, and Physical Properties of Selected Bituminous Coals and Cokes. Washington D.C.: U.S. Department of Interior, Bureau of Mines, Washington D.C. USA; 1979; p. 1-37.
[34] Badzioch S, Gregory DR, Field MA. Investigation of the temperature variation of thermal conductivity and thermal diffusivity of coal. Fuel 1964; 43: 267-280.
[35] Chin LY, Raghavan R, Thomas LK. Fully coupled geomechanics and fluidflow analysis of wells with stress-dependent permeability. SPE J. 2000; 5: 32-45.
[36] David C, Wong TF, Zhu W, Zhang J. Laboratory Measurement of Compaction-induced Permeability Change in Porous Rocks: Implications for the Generation and Maintenance of Pore Pressure Excess in the Crust. Pure Appl. Geophys. 1994; 143: 425-456.